Achieving High Selectivity for Alkyne Hydrogenation at High Conversions with Compositionally Optimized PdAu Nanoparticle Catalysts in Raspberry Colloid-Templated SiO_2

Mathilde Luneau[1], Tanya Shirman[2,3], Alexandre C. Foucher[4], Kaining Duanmu[5], David M.A. Verbart[1,6], Philippe Sautet[5,7], Eric A. Stach[4], Joanna Aizenberg[1,2,3], Robert J. Madix[2] and Cynthia M. Friend[1,2,*]

[1] Department of Chemistry and Chemical Biology, Harvard University, Cambridge, MA 02138, USA.
[2]John A. Paulson School of Engineering and Applied Sciences, Harvard University, Cambridge, MA 02138, USA.
[3] Wyss Institute for Biologically Inspired Engineering, Harvard University, Cambridge, MA 02138, USA.
[4] Department of Materials Science and Engineering, University of Pennsylvania, Philadelphia, PA 19104, USA
[5] Department of Chemical and Biomolecular Engineering, University of California, Los Angeles, CA 90095, US
[6] Inorganic Chemistry and Catalysis, Debye Institute for Nanomaterials Science, Utrecht University, Universiteitsweg 99, 3584 CG Utrecht, The Netherlands
[7]Department of Chemistry and Biochemistry, University of California, Los Angeles, CA 90095, US
*corresponding author: friend@harvard.edu

Abstract

Improving the selectivity for catalytic hydrogenation of alkynes is a key step in upgrading feedstocks for olefin polymerization. Herein, dilute Pd_xAu_{1-x} alloy nanoparticles embedded in raspberry colloid-templated silica (x=0.02, 0.04, and 0.09) are demonstrated to be highly active and selective for the gas-phase hydrogenation of 1-hexyne, exhibiting higher selectivity than pure Pd at high conversion. The conversion of 1-hexyne remains high even for the very low amounts of Pd in $Pd_{0.02}Au_{0.98}$. These catalysts are highly resistant to sintering—addressing a long-standing challenge in the use of Au-based catalysts. Clear evidence is presented that the addition of the second hydrogen to the half-hydrogenated intermediate is the rate-limiting step, and that the stability of the half-hydrogenated intermediate of the alkyne is higher than the half-hydrogenated alkene which explains the high selectivity even at high conversions. Moreover, of the three compositions investigated, optimum selectivity and activity is observed for the nanoparticles containing 4% Pd. The apparent activation energy for production of 1-hexene from 1-hexyne is measured to be 38 kJ mol^{-1} for the $Pd_{0.04}Au_{0.96}$ catalysts, which is ~14 kJ mol^{-1} lower than for pure Pd. The hydrogenation is completely, but reversibly, suppressed by adding CO to the reactant mixture, indicating that the Pd centers are the active sites for reaction. The method of templating used in preparation of the catalysts is highly customizable and versatile. This study demonstrates that the composition of the nanoparticles as defined by the dilution ratio of Pd in Au and by the method used to make the supported catalyst are important tunable parameters that can be used to optimize activity and selectivity of bimetallic systems.

Keywords: selective alkyne hydrogenation, dilute alloy catalysts, PdAu supported on SiO_2, colloidal templating, TEM, DFT

For Table of Contents Only

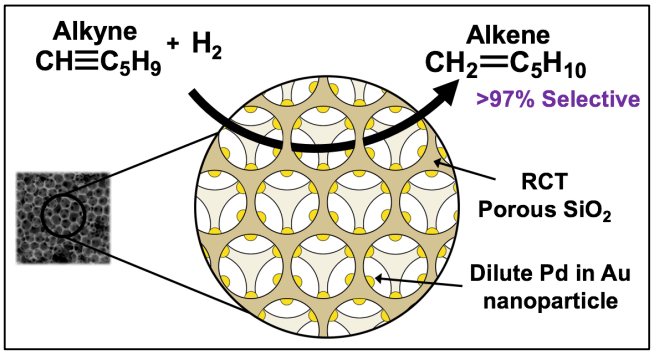

Introduction

Selective hydrogenation of alkynes (C≡C) to alkenes (C=C) without over-hydrogenation to alkanes is a key step in upgrading C_2-C_6 fractions from steam crackers.[1–3] Alkynes are generally present in trace amounts in industrial alkenes but act as poisons in downstream polymerization processes; hence, selective removal of the alkynes is critical.[1] The state-of-the-art catalyst system for this reaction remains the "Lindlar catalyst"[2] – a catalyst composed of high loadings of Pd (~5 wt.%) supported on CaCO3. It is also treated with quinolone and poisoned by toxic Pb to modulate activity and selectivity.[3] Nevertheless, the Lindlar catalyst has a selectivity substantially lower than desired; e.g. ~88% selectivity for production of 2-hexene from 2-hexyne at ~25% conversion[3] and only 0.02 wt.% of the total metal is estimated to be active during reaction.[4] Furthermore, the Pb additive is environmentally toxic.

The determining factors driving the selectivity for production of alkenes from alkynes over Pd at low conversions are thought to be: (1) a competitive hydrogenation of the alkyne versus the alkene; and (2) partial coverage of the Pd surface by adsorbates and oligomers. The competitive hydrogenation is generally explained by competition between the alkyne and alkene for active sites that is largely dictated by their respective heats of adsorption—alkynes bind more strongly to Pd than alkenes.[5–7] The stronger adsorption of the alkyne is proposed to be responsible for preventing adsorption of the alkene, which is a required step. Hence, alkyne adsorption and hydrogenation would dominate over the alkene as long as the conversion is not too high. Partial coverage of the Pd surface by adsorbates and oligomers would significantly decrease the number of available Pd sites, including larger Pd ensembles.[8] It is postulated that this site-blocking alters the performance of the Pd catalyst, leading to an increase in the selectivity accompanied by

a reduction in activity.[9] Although Pd is used commercially, there is great interest in identifying more selective catalysts, including very dilute PdAu alloys.[10–12]

Bimetallic Pd-based catalysts have been extensively studied as a potential means of increasing selectivity while preserving high conversions. Indeed, the selectivity for alkyne hydrogenation improves modestly with the addition of Cu (1 wt.%Pd - 1.2 wt.% Cu_2/Al_2O_3[13]), Ag (2.7 wt.% Pd - 5.5 wt.%Ag/Al_2O_3[14]) or Au (0.53 wt.% Pd - 1.15 wt.% Au/TiO_2[10] ; 0.1 wt.%Pd - 0.91 wt.%Au/TiO_2[11]). Improved selectivity for hydrogenation was also reported for catalysts prepared by dispersing single Pd atoms on graphene or modified graphene, but the conversion of the alkyne was not reported.[15,16] Finally, the single-atom alloy (SAA) approach combines the former and the latter strategies by atomically distributing Pd in a second metal such as Ag[17] or Au[12]. While the selectivity towards desired alkenes is enhanced by these methods, it is still well below 90%, and the activity is lower than that of monometallic Pd. Moreover, the effect of varying the Pd composition for the hydrogenation of acetylene in excess ethylene has been reported only for high Pd:Au and Pd:Ag atomic ratios (Pd:M atomic ratio >0.4[18]).

Herein, we report that the selectivity for hydrogenation of 1-hexyne (Fig. 1) is higher for highly dilute PdAu nanoparticles (NPs) than for pure Pd at high hexyne conversion. The conversion of 1-hexyne remains high even for very low amounts of Pd (Pd:Au atomic ratio < 0.1) in these novel catalysts. A novel catalyst architecture was used in which the Pd_xAu_{1-x} (x=0.02, 0.04, and 0.09) NPs are partially embedded in raspberry colloid templated (RCT)-SiO_2 (Fig. 2). These catalysts have the added benefit of being resistant to sintering after high-temperature treatment—addressing a long-standing challenge in the use of Au-based catalysts.[19] The materials synthesis method reported herein yields a robust catalyst system that can be customized by changing/tuning the nanoparticle and/or the support.[20] Thus, fine control over the composition, morphology, size and distribution of the supported nanoparticles is achieved.[21] We demonstrate here that such modular catalysts based on dilute Pd-in-Au nanoparticles embedded in RCT silica can be tuned to activate alkyne and hydrogen and selectively yield alkene. Furthermore, we show clear evidence that the addition of the second hydrogen to the half-hydrogenated intermediate is the rate-limiting step, and that the relative stabilities of the half-hydrogenated intermediates of the alkyne and alkene, respectively, explain the high selectivity for selective formation of hexene even at high conversions.

A key finding is that the $Pd_{0.04}Au_{0.96}$ RCT-SiO_2 has the optimum performance of the compositions studied. Specifically, the selectivity for alkene production is over 90% even at high conversion (80%), while preserving high activity.

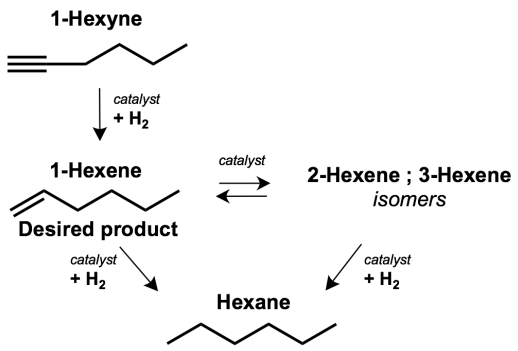

Figure 1: Schematic for catalytic hydrogenation of 1-hexyne. 1-Hexene is the desired product while all others are undesirable.

Materials and methods

Catalyst preparation

Catalysts were synthesized using a novel raspberry colloid-templating technique with three different nanoparticle compositions: $Pd_{0.02}Au_{0.98}$, $Pd_{0.04}Au_{0.96}$ and $Pd_{0.09}Au_{0.91}$.[19] Monometallic Au and Pd nanoparticles were synthesized for comparison purposes using a modified published method.[22] Monometallic Pd RCT-SiO_2 was prepared with 0.9 wt.% so that the Pd content was in the same order of magnitude as $Pd_{0.09}Au_{0.91}$ RCT-SiO_2. At lower loadings, there are risks of dispersions on the support after calcination at high temperature.[23] Pd_xAu_{1-x} nanoparticles were synthesized by addition of known volumes of Pd nitrate to a solution of Au nanoparticles (details in SI, S2).

Composite colloids were synthesized by adding specific amounts of Au, Pd_xAu_{1-x} or Pd nanoparticles to a colloidal dispersion of thiol-modified polystyrene colloids (S2.4). After formation of a colloidal assembly, a silica precursor was used to backfill interstitial space between the polystyrene spheres by capillary forces. Calcination at 500°C in air for two hours simultaneously removes the polymer colloids and organic volatiles, and solidifies the matrix into SiO_2.

Catalytic tests

Catalytic studies were carried out in a continuous-flow reactor at atmospheric pressure. Catalysts were crushed and sieved to obtain particle sizes between 100 and 300 μm. The

catalyst beds were prepared with 20 mg of pure Au or Pd_xAu_{1-x} RCT-SiO_2 and 10 mg of pure Pd RCT-SiO_2. A thermocouple was placed inside the catalyst bed. The catalysts were then mixed with quartz sand respecting a ratio of ~0.85 (volume quartz:volume quartz+catalyst) to minimize hot spot formation and loaded into a tubular quartz reactor tube (internal diameter: 1 cm). Gas phase 1-hexyne hydrogenation was carried out with a feed gas mixture of 1-hexyne (1%), H_2 (20%), in a balance of He at atmospheric pressure. The total flow rate was 50 mL min^{-1}, resulting in a gas hourly space velocity (GHSV) of 3,800 h^{-1}. Pretreatments in oxygen were carried out with 20% O_2 in He balance with a total flow rate 50 mL min^{-1} at 500°C for 30 min.
Experiments were started at low temperatures on the calcined catalysts. The temperature was then increased step by step, and steady-state conversions were reported. Reaction order studies were carried out at 40°C by varying the hydrogen inlet concentration between 5 to 20% at a fixed 1-hexyne concentration (1%). Reaction order of 1-hexyne was carried out by varying the 1-hexyne concentration (0.5 to 3%) at a fixed hydrogen concentration (20%). The effect of CO was studied by co-feeding CO to the standard reaction mixture at different temperatures. Steady state conversions were reported at various CO concentrations and reaction temperature over Pd and $Pd_{0.04}Au_{0.96}$ RCT-SiO_2. Apparent activation energies and reaction orders were determined considering reaction rates normalized by the amount of Pd at low conversion (≤ 20%) in a differential regime such that the difference between inlet and outlet concentrations can be directly related to the reaction rate.
Long-term stability tests were performed at 90°C on the calcined catalysts. Temperature programmed oxidation (TPO) was carried out after 22 hours of reaction over all Pd_xAu_{1-x}, Au and RCT-SiO_2 support and after 8 hours over Pd.

1-Hexene hydrogenation was carried out at 50°C after calcination over Pd and $Pd_{0.04}Au_{0.96}$ RCT-SiO_2 with a feed gas mixture of 1-hexene (1%), H_2 (20%) in a balance of He with a total flow rate of 50 mL min^{-1} at atmospheric pressure.

Catalytic performance was measured by effluent analysis using a GC/MS (Agilent Column HP-Plot/Q).

Carbon deposition was evaluated by performing TPO experiments after reaction using an online mass spectrometer with m/z = 4 for He, m/z = 18 for H_2O, m/z = 32 for O_2 and m/z = 44 for CO_2.

Density functional theory (DFT)

Pd(111) and Pd/Au(111) metal surfaces were modeled by using 6-layer metal slabs with 3x3 unit cell. The PBE functional[24] with dDSC dispersion correction was used, with cut-off energy of 400 eV, K-points was set to 7×7×1, the structure optimization threshold was 0.02 eV/Å. All calculations were performed with VASP.[25,26]

Results and Discussion

Catalyst preparation and characterization. The templating method yields Au, Pd_xAu_{1-x} or Pd particles embedded in silica (Fig. 2, S2 and S3). Before the templating approach, the average particle size was ~6 ± 2 nm for all three compositions ($Pd_{0.02}Au_{0.98}$, $Pd_{0.04}Au_{0.96}$ and $Pd_{0.09}Au_{0.91}$). The average particle size was preserved after calcination (Table 1). The average particle size was 4.8 ± 1.1 for the pure Pd RCT-SiO_2 after calcination, similar to that of the dilute Pd_xAu_{1-x} catalysts considering the standard deviation, and thus limiting potential particle size effect.[27,28] Assuming a 5 to 20% embedding of the $Pd_{0.04}Au_{0.96}$ nanoparticles in the RCT-SiO_2 support, the metal surface area is estimated to be around 1-10 m^2 g^{-1}.

Table 1: Self-standing nanoparticles size before the templating approach, size of nanoparticles embedded in RCT-SiO_2 and atomic Pd concentration of Au, Pd and Pd_xAu_{1-x} RCT-SiO_2

	Self-standing Nanoparticles	Nanoparticles embedded in RCT SiO_2 after calcination		Total metal loading
	Diameter (nm)[a]	Diameter (nm)[a]	atomic % Pd[b]	wt.%[b]
Au	5.1 ± 0.7	5.8 ± 1.2	0	4.5
$Pd_{0.02}Au_{0.98}$	5.4 ± 1.0	5.8 ± 1.4	2.1 ± 0.4	11.6
$Pd_{0.04}Au_{0.96}$	5.2 ± 0.9	6.0 ± 1.6	4.3 ± 0.2	2.5
$Pd_{0.09}Au_{0.91}$	5.8 ± 1.2	6.0 ± 2.1	9.5 ± 1.1	12.3
Pd	3.2 ± 0.8	4.8 ± 1.1	100	0.9

a. Average particle size as determined with TEM ; b. measured by ICP-MS

Pd retained its metallic state for all alloy compositions even though Pd is prone to oxidation in monometallic catalysts, based on ex situ XPS data (Fig. S4). Specifically, $Pd3d_{5/2}$ binding energies measured after calcination of $Pd_{0.04}Au_{0.96}$ and $Pd_{0.09}Au_{0.91}$ RCT-SiO_2 are 334.8 and 334.9 ± 0.1 eV, respectively, which is consistent with metallic Pd. For comparison, $Pd3d_{5/2}$ spectra are similar for clean Pd(111) (Fig S4).[29] The highly dilute

nature of the $Pd_{0.02}Au_{0.98}$ RCT-SiO_2 along with the overlap of the $Au4d_{5/2}$ and Pd3d renders it impossible to discern the oxidation state of Pd based on the XPS data; however, previous x-ray absorption spectroscopy (XAS) studies indicated Pd was predominantly metallic.[19,30] In the case of the monometallic Pd sample, $Pd_{5/2}$ appears at 336.4 ± 0.1 eV which corresponds to oxidized Pd species.[29,31]
The $Au4f_{7/2}$ region indicates a metallic state for all Au-containing catalysts based on the measured binding energies at 84.0 ± 0.1 eV (Fig S4).[32]

Prior studies using diffuse-reflectance infrared Fourier transform spectroscopy (DRIFTS) showed that Pd was atomically distributed on the surface of $Pd_{0.02}Au_{0.98}$ RCT-SiO_2 at room temperature after CO exposure, whereas both isolated and clustered atoms of Pd are present in $Pd_{0.09}Au_{0.91}$ RCT-SiO_2.[19] The data for the $Pd_{0.04}Au_{0.96}$ sample will be published in a separate study but the spectrum is essentially the same as $Pd_{0.02}Au_{0.98.}$ According to a previous XAS study, the majority of the Pd atoms are in the bulk of the Au nanoparticles after calcination and the surface Pd concentration is thus expected to be different than the bulk composition.[19] All catalysts were pretreated in the catalytic reactor in 20% O_2 in He balance at 500°C and cooled down in He before reaction to remove adventitious carbon and to create a uniform state of the material.

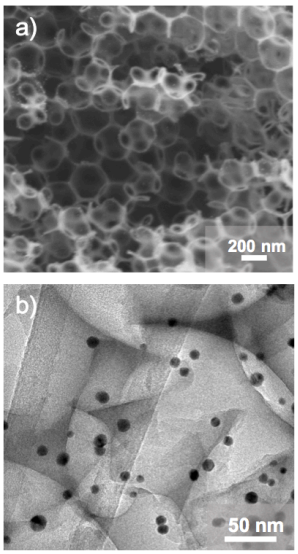

Figure 2: The Pd_xAu_{1-x} RCT-SiO_2 contain partially-embedded NPs in a highly structured SiO_2 matrix: a) Scanning electron microscopy (SEM) b) Transmission electron microscopy (TEM) of $Pd_{0.04}Au_{0.96}$ RCT-SiO_2.

All three alloy compositions embedded in the RCT-SiO_2 ($Pd_{0.02}Au_{0.98}$, $Pd_{0.04}Au_{0.96}$ and

$Pd_{0.09}Au_{0.91}$) were active for the hydrogenation of 1-hexyne to 1-hexene at 50°C (Fig. 3). Neither pure Au nanoparticles nor pure, metal-free, RCT-SiO_2 exhibited any detectable activity for hydrogenation of 1-hexyne (Figure S5). Assessment of the effects of diffusion using the Weisz-Prater and Carberry criteria indicate that mass transfer limitations under the reaction conditions employed were negligible (Table S1); indeed, internal mass transfer limitations were circumvented by the large size of the macropores (380 nm voids interconnected by 80 nm windows) in the silica matrix. The reliability of the preparation method was established by the reproducibility of the activity of catalyst observed over different batches of material with the same Pd_xAu_{1-x} composition (Fig. S6).

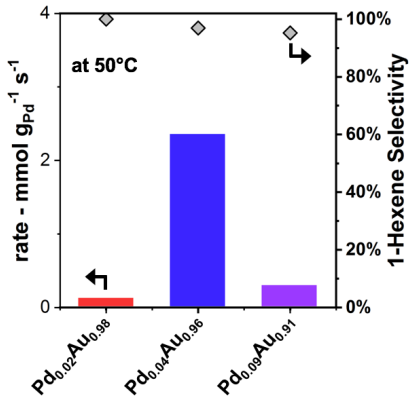

Figure 3: The rate of 1-hexyne conversion (▮) and the selectivity (◇) for 1-hexene production depend on the Pd content of the nanoparticles for $Pd_{0.02}Au_{0.98}$, $Pd_{0.04}Au_{0.96}$, $Pd_{0.09}Au_{0.91}$ at 50°C. Reaction conditions: 1% 1-hexyne, 20% H_2, He balance; m(Pd_xAu_{1-x} RCT-SiO_2) = 20 mg ; Total flow rate = 50 mL min^{-1} GHSV = 3,800 h^{-1}. Conversions: $Pd_{0.02}Au_{0.98}$, 0.4% $Pd_{0.04}Au_{0.96}$, 8.2% and $Pd_{0.09}Au_{0.91}$, 10.3%. All materials were pretreated in 20% O_2/He at 500°C *in-situ* before reaction.

The effects of alloy composition on rates and selectivity for 1-hexyne hydrogenation. The $Pd_{0.04}Au_{0.96}$ RCT-SiO_2 catalyst yielded the highest rate of 1-hexyne hydrogenation on a per Pd basis of the three bimetallic catalysts, while also maintaining >97% selectivity for 1-hexene production (Fig. 3). The rate at 50°C was an order of magnitude higher for $Pd_{0.04}Au_{0.96}$ RCT-SiO_2 than for either $Pd_{0.02}Au_{0.98}$ RCT-SiO_2, or $Pd_{0.09}Au_{0.91}$ RCT-SiO_2. Even with these high conversion rates, the selectivity for 1-hexene production was > 97% for the $Pd_{0.04}Au_{0.96}$ RCT-SiO_2 (Fig. 3). At iso-conversion, the yield to 1-hexene is much higher over $Pd_{0.04}Au_{0.96}$ RCT-SiO_2 than over other Pd_xAu_{1-x} and pure Pd RCT-SiO_2 catalysts (Fig. 4b).

Moreover, $Pd_{0.04}Au_{0.96}$ and $Pd_{0.09}Au_{0.91}$ showed significantly higher selectivity for the desired product 1-hexene than their pure Pd monometallic counterpart at high conversions (> 60%, Fig.4a). For the pure Pd catalyst the selectivity dropped to ~60% at high conversion while the $Pd_{0.04}Au_{0.96}$ catalyst maintained a selectivity of ~90% (Fig. 4a). $Pd_{0.02}Au_{0.98}$ is very selective, but such high conversions could not be achieved under the reaction conditions studied here due to the low concentration of active sites.

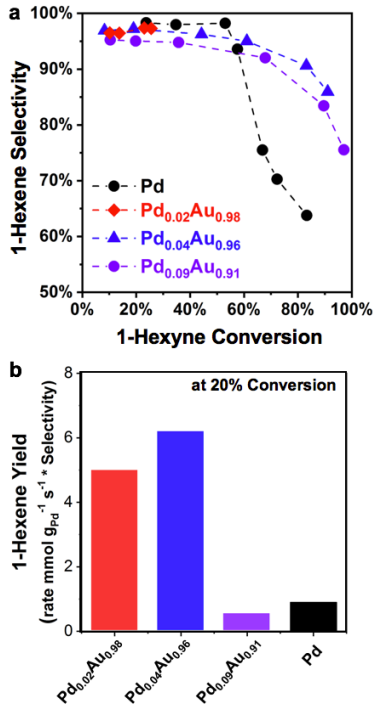

Figure 4: a) The selectivity for production of 1-hexene and the distribution of secondary products are different for pure Pd and Pd_xAu_{1-x} RCT-SiO_2 as shown by the comparison of the selectivity for 1-hexene production as a function of 1-hexyne conversion. 28 < T < 185°C b) $Pd_{0.04}Au_{0.96}$ RCT-SiO_2 shows the highest yield to 1-hexene compared to the other catalysts at iso-conversion (20%) ; T = 155, 75, 70 and 28°C over $Pd_{0.02}Au_{0.98}$, $Pd_{0.04}Au_{0.96}$, $Pd_{0.09}Au_{0.91}$ and Pd respectively. Reaction conditions: 1% 1-hexyne , 20% H_2, He balance ; m(Pd_xAu_{1-x} RCT-SiO_2) = 20 mg ; m(Pd RCT-SiO_2) = 10 mg ; Total flow rate = 50 mL min^{-1} ; GHSV = 3,800 h^{-1}

Clearly, the $Pd_{0.04}Au_{0.96}$ catalyst is superior to the other two Pd/Au compositions investigated. While the underlying reason for this variation is not yet established, the lower activity of $Pd_{0.09}Au_{0.91}$ RCT-SiO_2 is likely due to carbon deposition. (Carbon deposition is described in the ensuing section.) The lower activity of $Pd_{0.02}Au_{0.98}$ RCT-SiO_2 is ascribed to a lower concentration of the active Pd sites on the surface. The comparisons at iso-

temperature and iso-conversions indicate that differences in activation energies could be part of the explanation. Further investigation of these factors is underway.

The distribution of other products was also different for the reactions over pure Pd vs. Pd_xAu_{1-x} catalysts (Fig. 5). The main secondary product over pure Pd was hexane, while a mixture of hexene isomers (2-hexene and 3-hexene) formed over the Pd_xAu_{1-x} bimetallic catalysts. For instance, at ~80% conversion and using pure Pd RCT-SiO_2, hexane accounted for 21.8% of the products, while 2- and 3-hexene accounted for only 14.5%. Instead, 2- and 3-hexene isomers totaled to 5.4% of the products, hexane 3.9% of the undesirable secondary for the $Pd_{0.04}Au_{0.96}$ RCT-SiO_2 at the same conversion (Fig. 5).

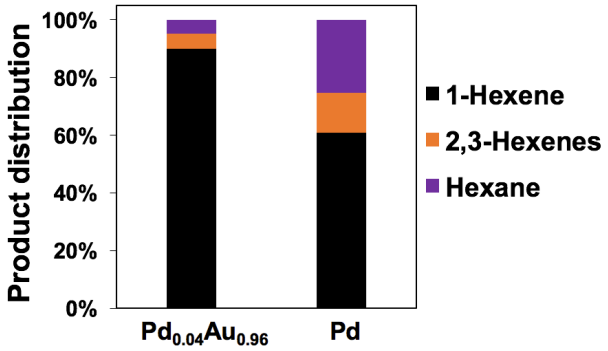

Figure 5: The product distribution is different at 83% conversion over $Pd_{0.04}Au_{0.96}$ (115°C) and pure Pd (50°C) ; Reaction conditions: 1% 1-hexyne , 20% H_2, He balance ; m($Pd_{0.04}Au_{0.96}$ RCT-SiO_2) = 20 mg ; m(Pd RCT-SiO_2) = 10 mg ; Total flow rate = 50 mL min^{-1} ; GHSV = 3,800 h^{-1}

Importantly, the catalytic performance of the $Pd_{0.04}Au_{0.96}$ RCT-SiO_2 was stable for more than 30 hours of operation at 90°C. It remained active (~50% conversion) and highly selective towards 1-hexene formation (~97%) during the total time-on-stream (Fig. 6), illustrating the high stability of the nanoparticle catalysts during reaction conditions after oxygen pre-treatment.

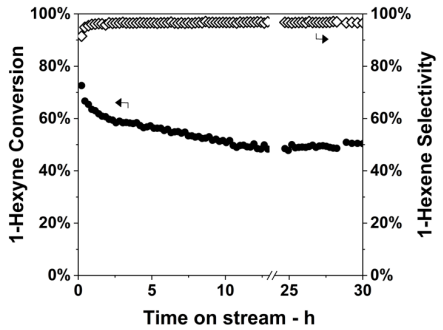

Figure 6: $Pd_{0.04}Au_{0.96}$ reaches stable conversion of 1-hexyne (●) and selectivity (◇) towards 1-hexene after calcination at 500°C in 20% O_2/He ; Reaction conditions: 1% 1-hexyne , 20% H_2, He balance T = 90° C ; m_{cat} = 20 mg ; Total flow rate = 50 mL min^{-1} ; GHSV = 3,800 h^{-1}

Carbon deposition under steady state conditions as a probe of the surface. Carbon was deposited during reaction on all catalysts investigated, based on TPO experiments performed after catalytic testing (Fig. 7). Carbon was detected through formation of CO_2 during temperature programmed oxidation. Different peak temperatures signify different forms of carbon. A single broad CO_2 peak was observed for oxidation of carbon deposited on Pd at 290°C. CO_2 was produced in a small broad peak at 380°C for the pure Au catalyst (Fig. 7). Notably, a single peak at ~350 °C was detected for the alloys with either 2 or 4 at.% Pd, whereas two peaks at 350 and 260°C were observed during TPO of the alloy catalyst containing 9 at.% Pd (Fig. 7). These data suggest that some of the carbon deposited on the alloy with 9% Pd is similar to that on pure Pd.

Carbon deposition is common during alkyne hydrogenation over Pd-based catalysts due to the formation of strongly bonded carbonaceous layer upon exposure to reaction conditions, as discussed above.[8,33] Indeed, build-up of carbonaceous species is thought to yield the undesirable byproduct, “green oil”, when Pd is used as a catalyst.[34] The TPO data suggest there are sufficiently large Pd clusters on the surface of the $Pd_{0.09}Au_{0.91}$ catalyst to imbue part of the surface with Pd-like reactivity, consistent with the previous work that shows clustering of Pd on the surface of this catalyst.[19] Additionally, since the catalysts with 2% and 4% Pd content catalyze oxidation of the adsorbed carbon fragments, O_2 can be dissociated at 300 – 350° C, even though clusters of Pd atoms could not be detected with CO DRIFTS.[19] The amount of CO_2 production in these experiments cannot be used to directly compare the amount of carbon deposited on the pure Pd vs. the alloys because the Pd was exposed to the 1-hexyne/H_2 reactant mixture for a shorter time and at a different reaction temperature.

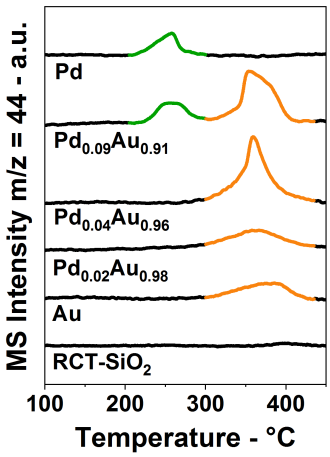

Figure 7. Deposition of carbon is demonstrated using temperature programmed oxidation (TPO) following hydrogenation of 1-hexyne using various NP RCT-SiO_2 catalysts. The CO_2 (m/z = 44) signal as a function of temperature is shown for Au, $Pd_{0.02}Au_{0.98}$, $Pd_{0.04}Au_{0.96}$, $Pd_{0.09}Au_{0.91}$ and pure Pd RCT-SiO_2. Essentially no CO_2 was observed over pure RCT-SiO_2 without NPs used as a control. The amount of CO_2 produced from the Pd catalyst is lower because it was on stream for a shorter time than the alloys. The data for all Pd_xAu_{1-x}, Au catalysts and pure RCT-SiO_2 were obtained after 22 hours on-stream at T = 90°C , whereas the TPO of Pd RCT-SiO_2 was performed after 8 hours on stream at 50°C. Reaction conditions: 1% 1-hexyne, 20% H_2, He balance; Total flow rate = 50 mL min^{-1}; GHSV = 3,800 h^{-1} - TPO Conditions: 20% O_2/He ; Total flow rate = 20 mL min^{-1} ; Ramp rate = 10°C min^{-1}

The structure of the catalyst and the size of the nanoparticles are preserved after high-temperature treatments and extended time on-stream. The used $Pd_{0.02}Au_{0.98}$, $Pd_{0.04}Au_{0.96}$ and $Pd_{0.09}Au_{0.91}$ RCT-SiO_2 showed no sintering after reaction and several calcinations as determined by *ex-situ* TEM performed after reaction (Fig. 8a and S7). Metallic Pd is still present at the surface of the nanoparticles after reaction as indicated by *ex-situ* XPS performed over used $Pd_{0.04}Au_{0.96}$ RCT-SiO_2 (Fig. S8). Further, there was no evidence of Pd or Au migration onto the silica from EDS-mapping (Fig 8c).This is a significant advance because Au-based catalyst are typically prone to sintering.[35] Leaching, which is sometimes reported for solution phase catalysis, is not viable under the conditions of these gas phase flow experiments. The $Pd_{0.04}Au_{0.96}$ RCT-SiO_2 is exceptionally resistant to sintering due to the novel catalyst architecture where nanoparticles are embedded in the SiO_2 host. More detailed studies of the Pd distribution in the $Pd_{0.04}Au_{0.96}$ RCT-SiO_2 catalysts are underway.

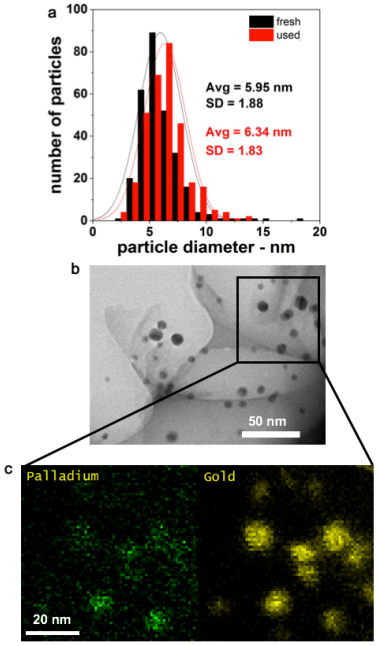

Figure 8: Post-reaction TEM analysis of used $Pd_{0.04}Au_{0.96}$ shows that: a) the average particle size is preserved after reaction and b) the structure of the silica remains intact. c) EDS-mapping indicates no migration of the Pd and Au to the silica support.

Poisoning by CO is reversible. The presence of CO in the reactant stream inhibited hydrogenation over $Pd_{0.04}Au_{0.96}$ and pure Pd at 50°C, indicating that the hydrogenation reaction depends on the availability of surface Pd. This conclusion is based on the fact that CO binds considerably more strongly on Pd (133 kJ mol^{-1}) than Au (44-54 kJ mol^{-1}), based on desorption measurements for Pd(111)[36] and roughened Au(111)[37]. On isolated Pd in Au, the desorption energy was measured to be ~80-84 kJ mol^{-1}.[12,38] CO was introduced at different partial pressures during reaction, and the steady state reaction rates dropped precipitously to nearly 0 with as little as 0.2% of CO co-fed with the reaction mixture (Fig. 9a). This effect is attributed to a competition for active sites between CO and the reactants and thus to a decrease in the number of sites available. This suggests that even though the active sites on $Pd_{0.04}Au_{0.96}$ and monometallic Pd are intrinsically different (isolated Pd atoms vs. extended surface), CO binds strongly on both with similar effects on reactivity.

As the reaction temperature was increased over $Pd_{0.04}Au_{0.96}$, the effect of CO addition became less pronounced. Significant hydrogenation of 1-hexyne was observed at 90 and 110°C in the presence of 0.2% CO, whereas the reaction was totally inhibited at 50 and 75°C (Fig. 9b). Estimations of the CO surface lifetime show a decrease from ~6 x 10^{-3} to

~6 x10^{-5} sec at 50 and 110°C respectively (assuming a desorption energy of 80 kJ mol^{-1} and a pre-exponential factor of 10^{15} s^{-1}).[12,36,39] This temperature dependence is thus attributed to a decrease in the steady state coverage of CO as a function of increasing temperature such that more active sites are available at the higher temperature. After exposure to different CO concentrations in the reactant stream, $Pd_{0.04}Au_{0.96}$ recovered its activity and selectivity within 30 minutes, corresponding to the time it takes for the reactor lines to be completely cleared out of CO, which further confirms that even very small concentrations of CO (<0.1%) poison the catalyst (Fig. S9). The CO-induced changes are thus reversible when CO is removed from the reactant gas stream at 50, 75, 90 and 110°C (the reversibility was not probed at 40°C). Thus, the presence of CO in the reactant gas does not seem to *irreversibly* alter the surface Pd concentration over this temperature range.

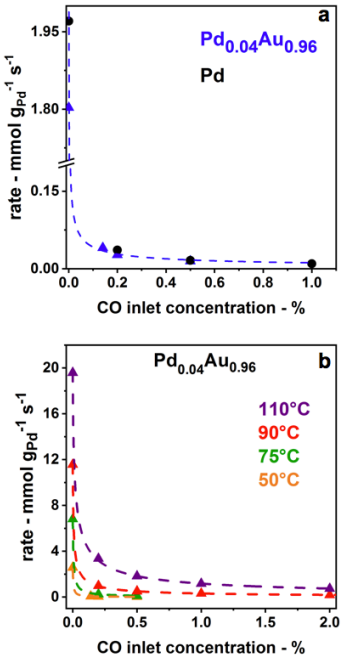

Figure 9: CO inhibits the selective hydrogenation of 1-hexyne over both pure Pd and $Pd_{0.04}Au_{0.96}$ RCT-SiO_2 catalysts. a) Steady-state rates after 30min of 1-hexyne conversion over pure Pd and $Pd_{0.04}Au_{0.96}$ at 50°C as a function of CO inlet concentrations show that CO inhibits the hydrogenation reaction. b) The effect of CO inlet concentrations on the rate of 1-hexyne conversion is less pronounced at higher temperature over $Pd_{0.04}Au_{0.96}$; Reaction conditions: 1% 1-hexyne , 20% H_2, 0-1% CO, He balance ; Total flow rate = 50 mL min^{-1} GHSV = 3,800 h^{-1}

Mechanistic considerations. The dependence of the rate of 1-hexyne hydrogenation on the partial pressure of reactants (Fig. 10) suggests that the reaction mechanism on

$Pd_{0.04}Au_{0.96}$ is similar to that on pure Pd, where the rate determining step is generally accepted to be addition of hydrogen to the adsorbed alkyne.[27,40] The most widely accepted and simplest reaction scheme for the hydrogenation of alkynes over Pd is the Horiuti-Polanyi mechanism.[41] In this mechanism, H_2 is dissociated and the alkyne molecularly adsorbs leading to a step-wise hydrogenation *via* a Langmuir-Hinshelwood path on the surface. Hydrogen atoms are added sequentially to the hydrocarbon intermediate followed by the desorption of the hydrogenated product.

Rate equations have been derived previously for several different reaction pathways with differing assumptions about the rate-determining step. The rate equation that is supported by our experiments (see below) for this mechanism has been derived previously (Eqn. 1).[27]

$$r_{alkyne} = -\frac{k'\, p_{H_2} p_{alkyne}}{\left(1+\sqrt{K_H p_{H_2}}+K_{alkyne} p_{alkyne}\right)^2} \quad (1)$$

$$with\ k' = k K_H K_{alkyne}$$

The derivation of this rate expression assumes that addition of the second H to the adsorbed, half-hydrogenated hexyne, with rate constant k, is the rate limiting step and that all other steps are (essentially) in equilibrium.

In the presence of 1-hexene and CO this equation becomes

$$r_{alkyne} = -\frac{k'\, p_{H_2} p_{alkyne}}{\left(1+\sqrt{K_H p_{H_2}}+K_{alkyne} p_{alkyne}+K_{alkene} p_{alkene}+K_{CO} p_{CO}\right)^2} \quad (2)$$

Since Eqn. 2 assumes that 1-hexene and CO compete for active sites, it reduces to Eqn. 1 when neither are present. The strong inhibiting effect of CO was noted above, consistent with this rate law (Fig. 9).

Both the conversion and selectivity for 1-hexene formation can be rationalized within the framework of the rate expression given by Eqn. 2. The reaction orders measured for hydrogen and 1-hexyne for both catalysts suggest that the active surface was largely covered with half-hydrogenated and adsorbed 1-hexyne and sparsely covered with H atoms.[42] The first-order dependence on p_{H2} indicates that $\sqrt{K_H p_{H_2}} \ll 1 + K_{alkyne} p_{alkyne}$ indicating that the equilibrium constant for hydrogen adsorption is sufficiently low to limit the hydrogen coverage. Further, for both the Pd and $Pd_{0.04}Au_{0.96}$ nanoparticle catalysts the rate was essentially independent of the 1-hexyne partial pressure (orders of -0.2 ±

0.02 for Pd and -0.08 ± 0.02 for $Pd_{0.04}Au_{0.96}$) (Fig. 10). This insensitivity reflects a large adsorption enthalpy indicative of the strong binding between the half-hydrogenated 1-hexyne intermediate and the active sites. On the other hand, according to Eqn. 1, the near independence of the reaction rate on 1-hexyne partial pressure indicates that the half-hydrogenated intermediate does not saturate the sites, in which case $K_{alkyne}p_{alkyne}$ would dominate the denominator, and the reaction order in 1-hexyne would become minus one. Such reaction orders are very comparable to studies performed with other alkynes over pure Pd and indicate that the competition of hydrogen with strongly bound 1-hexyne for active sites is largely dominated by the adsorbed hydrocarbon.[8,17,40]

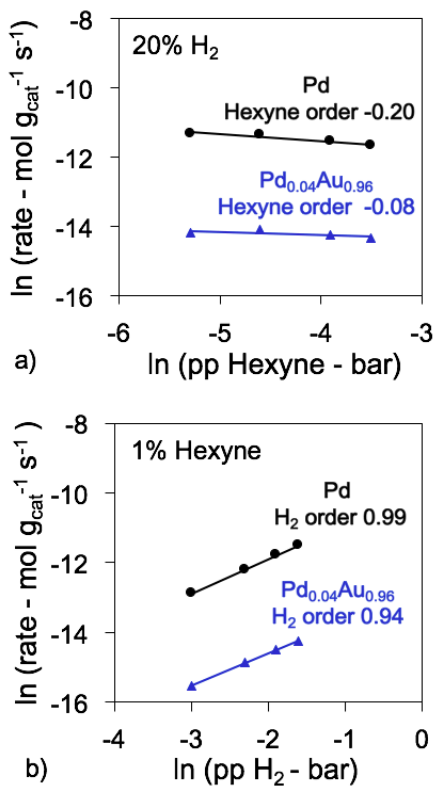

Figure 10: The reaction orders of 1-hexyne and hydrogen measured over $Pd_{0.04}Au_{0.96}$ and pure Pd indicate that the reaction mechanism does not significantly differ as shown by the reaction rate of 1-hexyne hydrogenation a) as a function of the partial pressure of 1-hexyne with fixed H_2 concentration and b) as a function of the partial pressure of hydrogen with fixed 1-hexyne concentration. Reaction conditions: He balance, T = 40° C; Total flow rate = 50 mL min^{-1} GHSV = 3,800 h^{-1}

The more negative reaction order in 1-hexyne observed for pure Pd suggests that 1-hexyne may be more strongly adsorbed on the active sites of Pd than on those of

$Pd_{0.04}Au_{0.96}$. DFT calculations show that acetylene and ethylene bind much more strongly on Pd than on dilute PdAu alloys, with adsorption energies for acetylene of -2.34 eV on Pd(111) and -0.85 eV on PdAu(111) and of -1.27 eV on Pd(111) and -0.75 eV on PdAu(111) for ethylene (Fig. 11). Similar orders of magnitude were reported on dilute PdAu systems.[43] In the literature, adsorption energies of C_2H_2 and C_2H_4 on Pd(111) were calculated to be -2.03 eV and -0.87 eV respectively with PW91 functional[44], which are weaker than calculations with dDSC dispersion correction used here.[45]

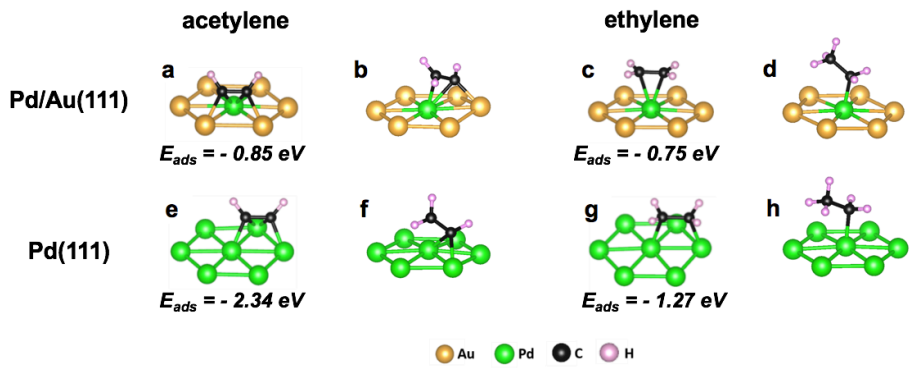

Figure 11: Adsorption energies (eV) of acetylene, ethylene and their partially hydrogenated fragments on dilute Pd/Au(111): (a) C_2H_2 in Pd-Au_2 3-fold hollow site ; (b) half-hydrogenated C_2H_3 bound to a Pd-Au bridge site (c) C_2H_4 in π mode over Pd and (d) half-hydrogenated C_2H_5 atop Pd. Parallel calculations yielded the structures and energies on Pd(111): (e) C_2H_2 in 3-fold hollow site; (f) half-hydrogenated C_2H_3 on a 2-fold bridge (g) C_2H_4 in di-σ mode over Pd_2 and (h) half-hydrogenated C_2H_5 atop Pd

The rate-determining step appears to be the addition of hydrogen to the adsorbed half-hydrogenated 1-hexyne for both the bimetallic alloy and pure Pd. DFT calculations are also supportive of this conclusion. The high selectivity for the partial hydrogenation of hexyne to hexene at high conversions suggests that the rate-limiting active intermediate for hexyne dominates the active sites. Indeed, DFT calculations for the equilibria between reactants and intermediates (hexyne/hexenyl and hexene/hexyl) indicate strong preference for the alkyne/alkenyl pair (Eqn. 3).

$$C_2H_{2,(gas)} + ½\ H_{2,(gas)} = C_2H_{3,(ads)} \quad \Delta E = -1.63\ eV \qquad (3)$$
$$C_2H_{4,(gas)} + ½\ H_{2,(gas)} = C_2H_{5,(ads)} \quad \Delta E = -0.95\ eV$$

The $Pd_{0.04}Au_{0.96}$ catalyst has a significantly lower apparent activation barrier. The apparent activation energy for 1-hexyne hydrogenation over $Pd_{0.04}Au_{0.96}$ is 38 ± 2 kJ mol^{-1}, 14 kJ mol^{-1} lower than either Pd RCT-SiO_2 (52 ± 0.4 kJ mol^{-1}) or of a physical mixture of monometallic Au and Pd RCT-SiO_2 with the same Pd:Au ratio (51 kJ mol^{-1}) (Fig. S10).

The measured value for pure Pd is in good agreement with the literature (Table 2).[17,18,46] Over Au supported on Al_2O_3 and CeO_2 apparent activation energy ranged between 34-37 kJ mol^{-1} for the hydrogenation of acetylene.[47,48] These data demonstrate that the $Pd_{0.04}Au_{0.96}$ RCT-SiO_2 catalyst is distinct from either Pd or Au. A more detailed investigation of the mechanisms for these hydrogenation processes is underway.

Table 2: Comparison of the apparent activation energies for selective hydrogenation to literature values for various Au, Pd and PdAu

catalyst	alkyne	$E_{a,app}$ – kJ mol^{-1}	Ref
$Pd_{0.04}Au_{0.96}$ RCT-SiO_2	1-hexyne	38	This work
Pd RCT-SiO_2	1-hexyne	52	This work
Au/Al_2O_3	acetylene	34	47
Au/CeO_2	acetylene	37	48
Au/SiO_2	1-hexyne	44.7	12
PdAu SAA/SiO_2	1-hexyne	46.7	12
Pd/SiO_2	acetylene	52	17
Pd/SiO_2	acetylene	51	18
Pd/C	1-hexyne	50	46

Selectivity at higher conversions of 1-hexyne. Insight into the difference in hydrogenation selectivity at the higher 1-hexyne conversions over the pure Pd and PdAu RCT-SiO_2 catalysts is provided by their respective catalytic behavior for hydrogenation of 1-hexene. They show a similarly high activity for conversion of 1-hexene to a mixture of hexene isomers and hexane at 50°C, indicating a similar ability for addition of adsorbed H to 1-hexene to form the adsorbed hexyl intermediate (the half-hydrogenated species) (Table S2). The striking difference between the two catalysts is that hexane is much more dominant for the pure Pd catalyst and the hexene isomers are the dominant product for the alloy catalyst. The implication therefore is that addition of the second H to form the alkane is more likely on the pure Pd catalyst than on the alloy, on which β-C-H bond breaking to reform one of the hexene isomers is preferred. Thus, at the high conversions of 1-hexyne on the catalysts significantly less formation of hexane would be expected on the alloy catalyst, as was observed experimentally (Fig. 4a).

Moreover, it appears that 1-hexene competes less favorably with 1-hexyne (or their half-hydrogenated counterparts) for surface sites on the alloy catalyst than on the pure Pd catalysts. Whereas hexene isomers and hexane form readily on the pure Pd catalyst,

there is less formation of hexene isomers and hexane on the alloy (Fig. 5), indicating that the half-hydrogenated hexyne dominates the alloy surface, ie, $K_{alkyne}p_{alkyne} > K_{alkene}p_{alkene}$. At equal gas-phase pressures of the two hydrocarbons $K_{alkyne} > K_{alkene}$. The logical deduction from this conclusion is that there is a change in the electronic structure of the Pd atom surrounded by the Au at the surface of the alloy that creates this difference in binding which is consistent with DFT calculations.

In summary, we suggest that a decrease in the adsorption energy of the unsaturated hydrocarbons on the alloy catalysts is the primary cause of its excellent selectivity. It must bind the alkyne strongly enough to allow it to react with adsorbed H, but bind the alkene weakly to favor its reversible desorption over its further hydrogenation. Recent studies over Pd-Ag catalysts show that ethylene transitions from strongly σ-bonded to π- bonded upon decreasing the concentration of Pd and thus the size of the Pd ensembles.[49] These findings may be transferable to our $Pd_{0.04}Au_{0.96}$ RCT-SiO_2 catalyst where the Pd is for the most part isolated in Au and the size of the Pd ensemble is thus very limited. A similar reduction of the binding energy of the half-hydrogenated intermediates relevant to the selective hydrogenation of 1-hexyne may play an important role. A full mechanistic study is underway to acquire a deeper understanding of the exceptional performances of $Pd_{0.04}Au_{0.96}$ RCT – SiO_2.

Comparison with other Pd bimetallic systems.

Other PdAu and PdAg bimetallic catalysts yielded between 38 to 50% selectivity at high conversions for acetylene in the gas phase, which is substantially lower than that measured here for the $Pd_{0.04}Au_{0.96}$ RCT SiO_2. Furthermore, the stability of these other catalysts at conversions lower than 100% was not assessed.[10,11,14] High conversions at high selectivities were achieved with bimetallic PdCu and single atom alloy (SAA) PdAg catalysts.[13,17] However, the reactions conditions used were substantially different than those used here—the PdCu catalyst was studied in the liquid phase (batch),[13] and the SAA PdAg in excess alkene.[17]

By the use of batch reactors Pd_xAu_{1-x} (x=0.004) nanoparticles supported on SiO_2 have been previously shown to be more selective than pure Pd nanoparticles for the liquid phase hydrogenation of 1-hexyne to hexane.[12] While the results are qualitatively similar to those reported here, significant differences suggest that the catalysts made with the raspberry colloid-templating method may be fundamentally different.

One notable difference is that the $Pd_{0.04}Au_{0.96}$ RCT-SiO_2 is more selective for production of 1-hexene in the gas-phase hydrogenation than the $Pd_{0.004}Au_{0.996}$ SAA catalyst supported on SiO_2 is for the liquid phase reaction. The selectivity for 1-hexene production on $Pd_{0.04}Au_{0.96}$ RCT-SiO_2 is ~97% at 50% conversion compared to ~85% for the $Pd_{0.004}Au_{0.996}$ SAA. A second important difference is that the apparent activation energies for hydrogenation of 1-hexyne for the two different systems are substantially different: 38 kJ mol^{-1} for the $Pd_{0.04}Au_{0.96}$ RCT-SiO_2 compared to 46.7 kJ mol^{-1} for the $Pd_{0.004}Au_{0.996}$ SAA. A variety of factors could account for this difference, including the higher H_2 pressure used in the liquid phase reactions, the larger particle size (7.58 ± 1.86 nm vs. 6 ± 1.6 nm vs.), the effect of solvent or fundamental differences in the catalyst materials, as discussed below. However, although both of these materials have atomically-dispersed Pd on the surface, these results suggest a fundamental difference between the two materials.

One key difference is the pretreatment methods employed in the two studies and their potential effect on the surface composition of the alloy nanoparticles. The Pd_xAu_{1-x} RCT SiO_2 catalysts were calcined at 500°C in their synthesis and again *in-situ* before being cooled to the reactor temperature and exposed to reactants in the flow reactor under reaction conditions to achieve steady state activity. In contrast, for the liquid phase studies the nanoparticles were first precipitated from solution, supported on silica by the introduction of fumed silica into the nanoparticles solutions, dried in vacuum for 24h and then subjected to hydrogen in the liquid phase reactor for one hour prior to the introduction of 1-hexyne. Studies of the $Pd_{0.04}Au_{0.96}$ RCT-SiO_2 catalysts in the gas phase reactor showed that treatment in H_2 in the gas phase suppresses the activity for gas phase hydrogenation of 1-hexyne. Hence, the calcining step in the preparation of the $Pd_{0.04}Au_{0.96}$ RCT-SiO_2, which is required to remove the colloid template, is an essential part of preparing very selective and active catalysts with low Pd content. Clearly the reductive treatment applied in the liquid phase may generate a significantly different surface composition from the oxidative treatment applied in the gas phase flow reactor, creating different catalyst activities.

Potential effects of subsurface hydrogen and carbon. It is important to also consider the possible contributions of subsurface hydrogen and carbon to the differences observed between the pure Pd and dilute PdAu NP catalysts. Previous work on pure Pd catalysts

suggests that the presence of Pd carbide and Pd hydride affect the activity and selectivity of acetylene hydrogenation. The hydride is more active and less selective, producing more alkane, whereas the surface carbide is less active but more selective. Their formation is highly dependent on reaction conditions and H_2/alkyne ratio.[50,51] These factors are unlikely to be operative on the dilute alloy catalysts, since the Pd atoms appear to be isolated at the surface. The existence of large ensembles of Pd, which would favor over-hydrogenation, could be eliminated by the high dispersion of Pd at the surface.[18] The lower concentration of Pd at the surface of the PdAu alloy should prevent the formation of a Pd hydride or carbide phase, and thus mitigate against over-hydrogenation.

Conclusions

All Pd_xAu_{1-x} RCT-SiO_2 catalysts proved to be more selective than their monometallic Pd counterpart and more active than monometallic Au for the selective hydrogenation of 1-hexyne towards 1-hexene. In agreement with prior studies, the presence of atomically dispersed Pd on the surface correlates with high selectivity for production of 1-hexene from 1-hexyne. Importantly, $Pd_{0.04}Au_{0.96}$ preserved high selectivity at high rates and conversions.

Oxygen pretreatment at high temperature leads to stable performances of $Pd_{0.04}Au_{0.96}$ RCT-SiO_2 over extended time on-stream. The high selectivity towards 1-hexene is attributed to a decrease in the binding strength of 1-hexene over diluted Pd in Au that prevents it from being over-hydrogenated to hexane even at high conversions. Here, we have shown that an optimum in concentration exists in a PdAu bimetallic system and lead to a synergy between activity and selectivity.

Author Contributions

CMF and RJM guided the research, PS, JA and ES participated to discussions. ML wrote the paper. TS designed and conducted the preparation of the materials, ML the flow reactor study and XPS, KD the DFT calculations, DV performed long-term stability tests, ACF the microscopy.

Supporting Information

The supporting information contains details about the synthesis of the materials, characterizations, control experiments, estimations of mass transfer limitations and arrhenius plots. This information is available free of charge on the ACS Publications website.

Acknowledgements

This work was supported as part of the Integrated Mesoscale Architectures for Sustainable Catalysis (IMASC), an Energy Frontier Research Center funded by the U.S. Department of Energy, Office of Science, Basic Energy Sciences under Award #DE-SC0012573. We thank Drs. Michael Aizenberg, Jeff Miller, Fang Xu and Mr. Christopher O'Connor for helpful discussions.

REFERENCES :

(1) Cardenas-Lizana, F.; Keane, M. A. The Development of Gold Catalysts for Use in Hydrogenation Reactions. *J. Mater. Sci.* **2013**, *48*, 543–564.

(2) Lindlar, H. Ein Neuer Katalysator Für Selektive Hydrierungen. *Helv. Chim. Acta* **1952**, *35*, 446–450.

(3) Schwab, F.; Weidler, N.; Lucas, M.; Claus, P. Highly Cis-Selective and Lead-Free Hydrogenation of 2-Hexyne by a Supported Pd Catalyst with an Ionic-Liquid Layer. *Chem. Commun.* **2014**, *50*, 10406–10408.

(4) Vilé, G.; Albani, D.; Almora-Barrios, N.; Lopez, N.; Pérez-Ramirez, J. Advances in the Design of Nanostructured Catalysts for Selective Hydrogenation. *ChemCatChem* **2016**, *8*, 21–33.

(5) Mei, D.; Sheth, P. A.; Neurock, M.; Smith, C. M. First-Principles-Based Kinetic Monte Carlo Simulation of the Selective Hydrogenation of Acetylene over Pd(111). *J. Catal.* **2006**, *242*, 1–15.

(6) Studt, F.; Abild-pedersen, F.; Bligaard, T.; Sørensen, R. Z.; Christensen, C. H.; Nørskov, J. K. Identification of Non-Precious Metal Alloy Catalysts for Selective Hydrogenation of Acetylene. *Science.* **2008**, *320*, 1320–1323.

(7) Sheth, P. A.; Neurock, M.; Smith, C. M. A First-Principles Analysis of Acetylene Hydrogenation over Pd(111). *J. Phys. Chem. B* **2003**, *107*, 2009–2017.

(8) Borodziński, A.; Bond, G. C. Selective Hydrogenation of Ethyne in Ethene-Rich Streams on Palladium Catalysts. Part 1. Effect of Changes to the Catalyst During Reaction. *Catal. Rev.* **2006**, *48*, 91–144.

(9) Zaera, F. The Surface Chemistry of Metal-Based Hydrogenation Catalysis. *ACS Catal.* **2017**, *7*, 4947–4967.

(10) Choudhary, T. V; Sivadinarayana, C.; Datye, A. K.; Kumar, D.; Goodman, D. W. Acetylene Hydrogenation on Au-Based Catalysts. *Catal. Letters* **2003**, *86*, 1–8.

(11) Mccue, A. J.; Baker, T.; Anderson, J. A. Acetylene Hydrogenation over Structured Au – Pd Catalysts. *Faraday Discuss.* **2016**, *188*, 499–523.

(12) Liu, J.; Shan, J.; Lucci, F. R.; Cao, S.; Sykes, E. C. H.; Flytzani-stephanopoulos, M. Palladium-Gold Single Atom Alloy Catalysts for Liquid Phase Selective Hydrogenation of 1-Hexyne. *Catal. Sci. Technol.* **2017**, *7*, 4276–4284.

(13) Markov, P. V; Bragina, G. O.; Rassolov, A. V; Baeva, G. N.; Mashkovsky, I. S.; Murzin, V. Y.; Zubavichus, Y. V; Stakheev, A. Y. Pd–Cu Catalyst Prepared from Heterobimetallic $PdCu_2(OAc)_6$: An XRD-EXAFS Study and Activity / Selectivity in the Liquid-Phase Hydrogenation of a C≡C Bond. *Mendeleev Commun.* **2016**, 502–504.

(14) Zhang, Q.; Li, J.; Liu, X.; Zhu, Q. Synergetic Effect of Pd and Ag Dispersed on Al_2O_3 in the Selective Hydrogenation of Acetylene. *Appl. Catal. A Gen.* **2000**, *197*, 221–228.
(15) Yan, H.; Cheng, H.; Yi, H.; Lin, Y.; Yao, T.; Wang, C.; Li, J.; Wei, S.; Lu, J. Single-Atom Pd_1/graphene Catalyst Achieved by Atomic Layer Deposition: Remarkable Performance in Selective Hydrogenaiton of 1,3-Butadiene. *J. Am. Chem. Soc.* **2015**, *137*, 10484–10487.
(16) Vilé, G.; Albani, D.; Nachtegaal, M.; Chen, Z.; Dontsova, D.; Antonietti, M.; López, N.; Pérez-Ramírez, J. A Stable Single-Site Palladium Catalyst for Hydrogenations. *Angew. Chemie - Int. Ed.* **2015**, *54*, 11265–11269.
(17) Pei, G. X.; Liu, X. Y.; Wang, A.; Lee, A. F.; Isaacs, M. A.; Li, L.; Pan, X.; Yang, X.; Wang, X.; Tai, Z.; Wilson, K.; Zhang, T. Ag Alloyed Pd Single-Atom Catalysts for Efficient Selective Hydrogenation of Acetylene to Ethylene in Excess Ethylene. *ACS Catal.* **2015**, *5*, 3717–3725.
(18) Zhang, Y.; Diao, W.; Williams, C. T.; Monnier, J. R. Selective Hydrogenation of Acetylene in Excess Ethylene Using Ag- and Au-Pd/SiO_2 Bimetallic Catalysts Prepared by Electroless Deposition. *Appl. Catal. A Gen.* **2014**, *469*, 419–426.
(19) Luneau, M.; Shirman, T.; Filie, A.; Timoshenko, J.; Chen, W.; Trimpalis, A.; Flytzani-Stephanopoulos, M.; Kaxiras, E.; Frenkel, A. I.; Aizenberg, J.; Friend, C.M.; Madix, R. J. Dilute Pd/Au Alloy Nanoparticles Embedded in Colloid Templated Porous SiO_2: Stable Au-Based Oxidation Catalysts. *Chem. Mater.* **2019**, *31*, 5759–5768.
(20) Shirman, E.; Shirman, T.; Shneidman, A. V; Grinthal, A.; Phillips, K. R.; Whelan, H.; Bulger, E.; Abramovitch, M.; Patil, J.; Nevarez, R.; Aizenberg, J. Modular Design of Advanced Catalytic Materials Using Hybrid Organic – Inorganic Raspberry Particles. *Adv. Funct. Mater.* **2017**, *1704559*, 1–20.
(21) Shirman, T.; Lattimer, J.; Luneau, M.; Shirman, E.; Reece, C.; Aizenberg, M.; Madix, R.; Aizenberg, J.; Friend, C. M. New Architectures for Designed Catalysts: Selective Oxidation Using AgAu Nanoparticles on Colloid-Templated Silica. *Chem. - A Eur. J.* **2017**, *24*, 1833–1837.
(22) Ding, Y.; Fan, F.; Tian, Z.; Wang, Z. L. Atomic Structure of Au−Pd Bimetallic Alloyed Nanoparticles. *J. Am. Chem. Soc.* **2010**, *132*, 12480–12486.
(23) Goodman, E. D.; Johnston-peck, A. C.; Dietze, E. M.; Wrasman, C. J.; Hoffman, A. S.; Abild-pedersen, F.; Bare, S. R.; Plessow, P. N.; Cargnello, M. Catalyst Deactivation via Decomposition into Single Atoms and the Role of Metal Loading. *Nat. Catal.* **2019**, *2*, 748–755.
(24) Perdew, J. P.; Burke, K.; Ernzerhof, M. Generalized Gradient Approximation Made Simple. *Phys. Rev. Lett.* **1996**, *77*, 3865–3868.
(25) Kresse, G.; Hafner, J. Ab Initio Molecular Dynamics for Liquid Metals. *Phys. Rev. B* **1993**, *47*, 558–561.
(26) Kresse, G.; Hafner, J. Ab Initio Molecular-Dynamics Simulation of the Liquid-Metal-Amorphous-Semiconductor Transition in Germanium. *Phys. Rev. B* **1994**, *49*, 14251–14269.
(27) Borodzinski, A.; Bond, G. C. Selective Hydrogenation of Ethyne in Ethene-Rich Streams on Palladium Catalysts. Part 2: Steady- State Kinetics and Effects of Palladium Particle Size, Carbon Monoxide, and Promoters. *Catal. Rev. Sci. Eng.* **2008**, *50*, 379–469.
(28) Tardy, B.; Noupa, C.; Leclercq, C.; Bertolini, J. C.; Hoareau, A.; Treilleux, M.; Faure, J. P.;

Nihoul, G. Catalytic Hydrogenation of 1,3-Butadiene on Pd Particles Evaporated on Carbonaceous Supports: Particle Size Effect. *J. Catal.* **1991**, *129*, 1–11.

(29) Lundgren, E.; Kresse, G.; Klein, C.; Borg, M.; Andersen, J. N.; Santis, M. De; Gauthier, Y.; Konvicka, C.; Schmid, M.; Varga, P. Two-Dimensional Oxide on Pd(111). *Phys. Rev. Lett.* **2002**, *88*, 246103.

(30) Timoshenko, J.; Wrasman, C. J.; Luneau, M.; Shirman, T.; Cargnello, M.; Bare, S. R.; Aizenberg, J.; Friend, C. M.; Frenkel, A. I. Probing Atomic Distributions in Mono- and Bimetallic Nanoparticles by Supervised Machine Learning. *Nano Lett.* **2019**, *19*, 520–529.

(31) Gabasch, H.; Unterberger, W.; Hayek, K.; Klotzer, B.; Kleimenov, E.; Teschner, D.; Zafeiratos, S.; Ha, M.; Knop-Gericke, A.; Schlogl, R.; Han, J.; Ribeiro, F. H.; Aszalos-Kiss, B.; Curtin, T.; Zemlyanov, D. In Situ XPS Study of Pd(111) Oxidation at Elevated Pressure, Part 2: Palladium Oxidation in the 10^{-1} mbar Range. *Surf. Sci.* **2006**, *600*, 2980–2989.

(32) Seah, M. P.; Gilmore, I. S.; Beamson, G. XPS: Binding Energy Calibration of Electron Spectrometers 5 - Re-Evaluation of the Reference Energies. *Surf. Interface Anal.* **1998**, *26*, 642–649.

(33) Molnar, A.; Sarkany, A.; Varga, M. Hydrogenation of Carbon – Carbon Multiple Bonds: *J. Mol. Catal. A Chem.* **2001**, *173*, 185–221.

(34) Vignola, E.; Steinmann, S. N.; Farra, A. Al; Vandegehuchte, B. D.; Curulla, D.; Sautet, P. Evaluating the Risk of C−C Bond Formation during Selective Hydrogenation of Acetylene on Palladium. *ACS Catal.* **2018**, *8*, 1662–1671.

(35) Olmos, C. M.; Chinchilla, L. E.; Delgado, J. J.; Hungría, A. B.; Blanco, G.; Calvino, J. J.; Chen, X. CO Oxidation over Bimetallic Au-Pd Supported on Ceria-Zirconia Catalysts: Effects of Oxidation Temperature and Au:Pd Molar Ratio. *Catal. Letters* **2016**, *146*, 144–156.

(36) Guo, X.; Yates Jr, J. T. Dependence of Effective Desorption Kinetic Parameters on Surface Coverage and Adsorption Temperature: CO on Pd(111). *J. Chem. Phys.* **1989**, *90*, 1.

(37) Yim, W.; Nowitzki, T.; Necke, M.; Schnars, H.; Nickut, P.; Biener, M. M.; Zielasek, V.; Al-shamery, K.; Ba, M. Universal Phenomena of CO Adsorption on Gold Surfaces with Low-Coordinated Sites. *J. Phys. Chem. C* **2007**, 111, 445–451.

(38) Gao, F.; Wang, Y.; Goodman, D. W. CO Oxidation over AuPd(100) from Ultrahigh Vacuum to Near-Atmospheric Pressures: CO Adsorption-Induced Surface Segregation and Reaction Kinetics. *J. Phys. Chem. C* **2009**, No. 100, 14993–15000.

(39) Lucci, F. R.; Darby, M. T.; Mattera, M. F. G.; Ivimey, C. J.; Therrien, A. J.; Michaelides, A.; Stamatakis, M.; Sykes, E. C. H. Controlling Hydrogen Activation, Spillover, and Desorption with Pd−Au Single-Atom Alloys. *J. Phys. Chem. Lett.* **2016**, *7*, 480–485.

(40) Brandao, L.; Fritsch, D.; Mendes, A. M.; Madeira, L. M. Propyne Hydrogenation Kinetics over Surfactant-Stabilized Palladium Nanoclusters. *Ind. Eng. Chem. Res.* **2007**, *46*, 377–384.

(41) Horiuti, I.; Polanyi, M. Exchange Reactions of Hydrogen on Metallic Catalysts. *Trans. Faraday Soc.* **1934**, *30*, 1164–1172.

(42) Boudart, M. *Kinetics of Chemical Processes*; Butterworth-Heinemann, Ed.; 1991.

(43) Liu, J.; Uhlman, M. B.; Montemore, M. M.; Trimpalis, A.; Giannakakis, G.; Shan, J.; Cao,

S.; Hannagan, R. T.; Sykes, E. C. H.; Flytzani-stephanopoulos, M. Integrated Catalysis-Surface Science-Theory Approach to Understand Selectivity in the Hydrogenation of 1-Hexyne to 1-Hexene on PdAu Single-Atom Alloy Catalysts. *ACS Catal.* **2019**, *9*, 8757–8765.

(44) Mittendorfer, F.; Thomazeau, C.; Raybaud, P.; Toulhoat, H. Adsorption of Unsaturated Hydrocarbons on Pd(111) and Pt(111): A DFT Study. *J. Phys. Chem. B* **2003**, *107*, 12287–12295.

(45) Steinmann, S.; Corminboeuf, C. A Generalized-Gradient Approximation Exchange Hole Model for Dispersion Coefficients. *J. Chem. Phys.* **2011**, *134*, 44117.

(46) Semagina, N.; Renken, A.; Kiwi-Minsker, L. Monodispersed Pd-Nanoparticles on Carbon Fiber Fabrics as Structured Catalyst for Selective Hydrogenation. *Chem. Eng. Sci.* **2007**, *62*, 5344–5348.

(47) Jia, J.; Haraki, K.; Kondo, J. N.; Domen, K.; Tamaru, K. Selective Hydrogenation of Acetylene over Au/Al_2O_3 Catalyst. *J. Phys. Chem. B* **2000**, *104*, 11153–11156.

(48) Azizi, Y.; Petit, C.; Pitchon, V. Formation of Polymer-Grade Ethylene by Selective Hydrogenation of Acetylene over Au/CeO_2 Catalyst. *J. Catal.* **2008**, *256*, 338–344.

(49) Li, M.; Shen, J. Microcalorimetric and Infrared Spectroscopic Studies of CO and C2H4 Adsorption on Pd/SiO2 and Pd–Ag/SiO_2 Catalysts. *Mater. Chem. Phys.* **2001**, *68*, 204–209.

(50) Teschner, D.; Borsodi, J.; Wootsch, A.; Révay, Z.; Hävecker, M.; Knop-gericke, A.; Jackson, S. D.; Schlögl, R. The Roles of Subsurface Carbon and Hydrogen in Palladium-Catalyzed Alkyne Hydrogenation. *Science.* **2008**, *320*, 86–90.

(51) Zhao, S.; Li, Y.; Liu, D.; Liu, J.; Liu, Y.; Zakharov, D. N.; Wu, Q.; Orlov, A.; Gewirth, A. A.; Stach, E. A.; Nuzzo, R. G.; Frenkel, A. I. Multimodal Study of the Speciations and Activities of Supported Pd Catalysts During the Hydrogenation of Ethylene. *J. Phys. Chem. C* **2017**, *121*, 18962–18972.